EUROPEAN ORGANIZATION FOR NUCLEAR RESEARCH

NP Internal Report 70-4
February 19, 1970.

TOTAL AND ABSORPTION CROSS SECTIONS OF π^-, K^- AND $\bar{p}$ IN THE MOMENTUM RANGE 20-65 GeV/c.

J.V. Allaby*), Yu.B. Bushnin+), S.P. Denisov+), A.N. Diddens*), R.W. Dobinson*), S.V. Donskov+), G. Giacomelli†), Yu.P. Gorin+), A. Klovning*), A.I. Petrukhin+), Yu.D. Prokoshkin+), R.S. Shuvalov+), C.A. Stahlbrandt*), D.A. Stoyanova+)

IHEP-CERN Collaboration
Institute for High-Energy Physics, Serpukhov, USSR.

A B S T R A C T

Total cross-section data are presented for negative pions, kaons, and antiprotons on protons and deuterons in the momentum range 20 GeV/c to 65 GeV/c in 5 GeV/c steps. Absorption cross-sections are given for the same particles on nine nuclei (He, Li, Be, C, Al, Cu, Sn, Pb and U) in the same momentum range.

English version of a paper
submitted for publication to
Yadernaya Fisika
December 1969

---

*) CERN, Geneva, Switzerland.
+) IHEP, Sepukhov, USSR.
†) Visitor at CERN from the University of Bologna and INFN Bologna, Italy.

1. Introduction

Detailed studies of total cross-sections for the interactions of hadrons with protons and neutrons, made during the last few years with energies up to ~30 GeV[1-5], have resulted in precise information on the properties of hadrons and the characteristics of strong interactions. Results of total cross-sections at low energies have led to the discovery of a series of new resonances[1-2]. At higher energies, where the effects of resonances are no longer important, the energy dependence of the cross-sections and the relations between the cross-sections for different particles are of great interest. In the case of the energy dependence of total cross-sections, there exists a large number of theoretical models, usually in the framework of Regge-pole theory[6-11]. For relationships between cross-sections, it is supposed that at very high energies the total cross-sections of particles and antiparticles should become equal according to the Pomeranchuk theorem[12] and should not depend on isotopic spin[13]. In addition, the ratios between πN, KN and NN cross-sections can be predicted on the basis of the quark model[14].

Measurements of absorption cross-sections of hadrons on nuclei at high energy are also of interest. Comparison of such results with theoretical calculations[15-17], give the opportunity to verify our understanding of the interactions of hadrons at high energies with nuclear matter and to obtain information on the properties of nuclei.

This article describes an experiment to measure total cross-sections, σ_{tot}, and absorption cross-sections, σ_{abs}, for π^-, K^- and antiprotons in the new energy region accessible at the 70 GeV accelerator of IHEP. Some of the results have already been published[18]. The scope of the measurements is shown in table 1.

The technique of measurement is described in section 2, the experimental equipment in section 3, the experimental procedure in section 4, and data analysis in section 5. The derivation of cross-sections on neutrons and of cross-sections for definite isotopic spin states are dealt with in section 6. In section 7 the results of the total cross-sections are discussed. Section 8 is devoted to a discussion of the results of absorption cross-sections on atomic nuclei.

2. The Principle of the Measurement.

For the measurement of total cross-sections the transmission technique was used in conditions of "good geometry"[1-3]. The principle of this method of measurement is illustrated in Fig. 1a). In the path of a focussed beam of primary particles are positioned the target G and the counter S, which measures the particle flux M, incident on the target. Near the focus of the beam a series of transmission counters T_i are placed which subtend different angles Θ_i with respect to the centre of the target. If the target is in the beam, the number of particles N_{if}, registered by the counter T_i, divided by the incident flux M_f given by the counter S, is determined by the following relation:

$$N_{if}/M_f = g_i \exp(-n\sigma_i) \qquad (1)$$

where n is the number of nuclei per cm^2 in the target and the partial cross-section σ_i is related to the total cross-section in the following way :

$$\sigma_i = \sigma_{tot} - \sum_K \int_{\Omega_i} d\Omega \; \frac{d\sigma_K(\Theta)}{d\Omega} \qquad (2)$$

The factor g_i in equation (1) takes account of the efficiency of the equipment and the loss of beam particles by interaction or decay between the counters S and T_i, excluding the absorption in the target itself. The differential cross-section $(d\sigma_K/d\Omega)$

in equation (2) represents the angular distribution of charged secondaries for a reaction channel K (the sum is over all possible channels).

If it is assumed that the probability of interaction or decay between the target and the counter T_i and the detection efficiency of the equipment, are independent of the presence or absence of the target in the beam (neglecting the effects of energy loss in the target), then:-

$$g_i = N_{ie}/M_e \qquad (3)$$

where the subscript e refers to measurements without the target. From (1) - (3) it follows that the total cross-section may be obtained by an extrapolation of the partial cross-sections

$$\sigma_i = \frac{1}{n} \ln \frac{N_{ie}/M_e}{N_{if}/M_f} \qquad (4)$$

to $\Theta_i = 0$.

From (2) it follows that the angular distributions $d\sigma_K/d\Omega\ (\Theta)$ of all the processes which make up the total cross-section measured must be much wider than the range of values of Θ_i chosen for the extrapolation. On the other hand, if for some reaction channel the angular distribution is concentrated in the range $0 \leq \Theta \leq \Theta_1$ it will not be counted in the σ_{tot} measured. This fact is used to separate the strong and electromagnetic processes in the measurement of total cross-sections of elementary particles on protons and deuterons: the angle of acceptance Θ_1 of the first transmission counter ring may be chosen so that it accepts fully the narrow peak of coulomb scattering and the coulomb-nuclear interference, and at the same time that it accepts only a small part of the strong interaction processes. However, the angular distribution of diffraction scattering of particles on heavy nuclei is such that a large fraction occurs in the region of coulomb scattering and one cannot obtain the "good geometry" situation. In this case the magnitude of Θ_1 is chosen such that

the counter T_1 accepts not only the coulomb scattering but also the nuclear elastic diffraction scattering. For this reason, for heavy nuclei, the quantity measured is not the total cross-section but the absorption cross-section $\sigma_{abs} = \sigma_{tot} - \sigma_{el}$ where σ_{el} is the total elastic cross-section. Since the range of extrapolation is larger than in the case of a determination of σ_{tot} on hydrogen or deuterium, and since the formula to be used for the extrapolation is not known, the systematic errors of such a determination of the nuclear absorption cross-sections will be larger.

The choice of the extrapolation range is determined not only by the angular distributions $d\sigma_K/d\Omega$, but also by the dimensions of the beam at the focus. This point will be examined in detail in section 4.

Below, in place of Θ, the four-momentum transfer squared t will be used. For $\Theta \ll 1$, $|t| \approx p^2\Theta^2$ where p is the momentum of the incident particles.

3. Experimental Layout and Equipment.

The plan of the experiment is shown in Fig. 1b. The accelerated proton beam was directed onto one of three aluminium targets placed inside the vacuum chamber of the accelerator. Negatively charged secondary particles, emerging at small angles from the target, were deflected by the magnetic field of the accelerator and passed into the beam transport system[19]. For secondary momenta p from 40-65 GeV/c the protons were accelerated up to an energy of 70 GeV; in the measurements of total cross-sections at lower momenta, the energy of the primary protons was 52, 43 and 35 GeV respectively. The momentum acceptance of the beam, Δp, was determined by the size of the momentum slit K_3. Normally an aperture of 12 mms was used corresponding to $\Delta p/p = \pm 1\%$. For particle identification, a dispersion compensated differential Cerenkov counter D[19] was used, placed in a parallel section of the beam, and a high resolution threshold Cerenkov

counter $\check{C}^{20}$). The lenses L_8-L_{10} focussed the beam on the first transmission counter T_1. The position of the beam spot at the transmission counters could be optimized with the aid of the magnets M_3 (horizontally) and M_4 (vertically) and was checked during the experiment using the scintillation counters S_4 and S_5 with diameters 1 cm and 3 cm respectively.

The flux of particles incident on the target was determined by the scintillation counters S_1, S_2 and S_3 with diameters 8, 8 and 5 cms respectively. The anti-coincidence counters A_1 and A_2, each with a central hole, reduced the background level caused by the interactions of the beam "halo" with the walls of the differential Čerenkov counter and the target.

For the identification of π-mesons in the beam, the threshold Čerenkov counter $\check{C}$ was used with the output in coincidence with the signal $M_0 = S_1 S_2 S_3 \bar{A}_1 \bar{A}_2$. K^--mesons and antiprotons were identified using the differential Čerenkov counter D, (see fig. 2), whilst the threshold counter was connected in anticoincidence to reduce the background from lighter particles to a level of less than 0.1%. In this case the monitor signal used was $M = M_0 D\bar{\check{C}}$. Typical counting rates of the monitor M per machine cycle were $\sim 10^4\ \pi^-$, $\sim 10^3 K^-$, $\sim 10^2 \bar{p}$, with a burst length of $\approx$ 0.5 sec.

In the experiment, 3 m long gas targets were used containing hydrogen, deuterium and helium at a pressure of $\approx$ 70 atmospheres and at liquid nitrogen temperature ($\approx$ 78°K) (see fig. 3). Under these conditions, the quantity of gas in the beam was $\approx$ 7 gm cm^{-2} of hydrogen and $\approx$ 14 gm cm^{-2} of deuterium and helium. The total thickness of the spherical windows of the targets, constructed of stainless steel, was $\approx$ 2 gm cm^{-2}. For the measurements with an "empty" target an identical target was used evacuated to a pressure of 10^{-2} Torr. The gas pressure in the targets was measured with a precision of $\pm$0.1 atmosphere using manometers which were calibrated before and after each run. The temperature of the targets was determined to an accuracy of $\pm$0.5°K by the constant volume gas thermometer technique. The evaluation of the hydrogen density

from the measured temperature and pressure was carried out using the equation of state as given by Rabinovich[21]. This method gives agreement with experimental data[22,23] to within ±0.2%. The deuterium density was calculated from the data of Michels et al[23] which, however, had to be extrapolated to lower temperature. This was done using the Beattie-Bridgman[24] equation of state, which was also used for the calculation of the helium density. The precision of the density determination described was ± 0.7% for hydrogen and helium, and ±0.9% for deuterium. The experimental checks of the total cross-sections of π^--mesons using the CH_2 -C difference technique, and using the gas targets at room temperature, proved the reliability of the procedure used for the density evaluations.

For the measurements of absorption cross-sections targets of diameter 130 mm and thicknesses from 6 to 34 gm cm^{-2} were used (Table 2).

Twelve circular transmission counters were mounted on a trolley which could move along rails along the beam. The dimensions of the scintillators are shown in Table 3. For each momentum of incident particles, the distance of the transmission counters from the centre of the target was chosen such that the counter T_6 accepted a fixed maximum four momentum transfer squared $|t| \leq 0.038$ (GeV/c^2). This was done to minimize energy-dependent systematic errors in the extrapolation of the partial cross-sections to t = 0 (see below). For the momenta 20 and 25 GeV/c the trolley could not be moved sufficiently close to the target to satisfy this condition, and thus the counters were placed at the minimum distance possible. In order to eliminate possible errors which might be caused by detection of particles passing only through the plexiglass light-guides of the transmission counters, neighbouring counters were mounted on the common supporting framework in such a way that their light guides did not overlap, and the signal from counter i was put in coincidence with that from counter i+1, to make the logic signal Q_i.

The two small counters S_4 and S_5 were mounted on the same line as the transmission counters.

The horizontal and vertical intensity distribution at the beam focus was measured by the pulse height distribution from the wedge-shaped scintillation detectors W [25] placed in front of the counter S_4 and connected in coincidence with the signal M_o. The calibration of the detector W was made using the coincidence $M_o W\ S_4\ S_5$. The calibration curve represented the pulse-height distribution from the detector W for a beam with diameter 1 cm (dimension of counter S_4), passing along the axis of the transmission counters. When the maximum of the calibration curve and the beam profile curve were coincident, the beam passed through the centres of the transmission counters T_i (this also corresponded to the maximum coincidence rate of $M_o\ S_4\ S_5$ as a function of the currents in magnets M_3 and M_4). The comparison of the widths of the two curves gives an estimate of the size of the beam spot at the focus. In fig. 4 are shown typical distributions obtained during the measurements of the beam profile and calibration curves. The full width at half height of the transverse beam dimensions was typically ~ 2 cm.

Behind the transmission counters two blocks of steel absorber were placed, each 1.5 m thick, and the two scintillation counters S_6 and S_7 which were used for measurements of the muon-contamination in the beam.

A simplified electronic logic diagram is shown in Fig. 5. The signals of the monitors M_o and M, and the signal from the coincidence between neighbouring transmission counters $Q_i = T_i\ T_{i+1}$ were used to form three types of coincidence: $M\ Q_i$, $M_o Q_i\ S_4\ S_5$ and $M\text{-}Q_i$. From the counting rate $M\ Q_i$, the flux detected by the i^{th} counter was determined, the coincidence $M_o Q_i\ S_4\ S_5$ checked the efficiency of channel i, and the $M\text{-}Q_i$ delayed coincidence determined the accidental coincidences in the monitor for a delay equal to one R.F. period (165 n sec).

The electronic dead time, equal to 45 n sec, was set by the pulse shaping circuits of counters S_1 and S_2.

4. Measurement Procedure

The experimental data were obtained during four experimental periods on the accelerator. During each run, the total cross-section for π^--mesons was measured at 40 GeV/c to check the reproducibility of the results. The total data for each momentum and for each particle were gathered in a cyclic series of measurements of the targets: hydrogen, deuterium, helium and "empty" and similarly for the complex nuclei. The number of counts MQ_i, $M_oQ_iS_4S_5$ and $M\text{-}Q_i$ were recorded for a given number of monitor counts M. After each measurement, the data were punched onto cards for off-line analysis using the MINSK-22 computer. For each measurement it was checked that the efficiency of the counters were always better than 99.5%, and the delayed coincidences were less than 1% (2% for antiprotons). During the measurements at 40 GeV/c, the beam intensity was raised and lowered by a factor of three compared with the normal value. This showed that, within the statistical errors, such a change in beam intensity had no effect on the cross-section measured. During other control measurements, it was shown that reducing the gas density in the hydrogen, deuterium and helium targets by a factor 4, or changing the thickness of the carbon target from 13.1 gm cm^{-2} to 40.5 gm cm^{-2} made no change in the results obtained for the cross-sections. The absorption produced by the target end windows was shown to be equivalent to the absorption of the dummy cell by measurement with the target cells evacuated.

5. Calculation of the cross-sections

The total cross-sections σ_{tot} were evaluated by extrapolation of the partial cross-sections to t = 0 (see section 2). For the extrapolation the following parametrisation was used:

$$\sigma_i = \sigma_{tot} \exp (at_i + b\, t_i^2) \qquad (5)$$

were the parameters σ_{tot}, a and b were obtained from a least-squares fit. For the calculation of the total cross-sections on H_2 and D_2, ususally the partial cross-sections measured by the counters T_3 - T_8 were used, which corresponded to an interval

of $0.014 \leq |t| \leq 0.065$ $(GeV/c)^2$. The partial cross-sections σ_1 and σ_2 contained a non-negligible contribution from multiple coulomb scattering and thus were not taken into consideration in the evaluation of σ_{tot}. To estimate the systematic error associated with this extrapolation procedure, the total cross sections were evaluated by adding or subtracting one transmission counter from either end of the extrapolation range. The spread of the five values of σ_{tot} obtained in this way was taken into account in the error estimation of the experimental results. The parameter a in equation (5) was rather momentum independent and well determined. Typical values are 3.5, 3.2, and 4.5 GeV/c^{-2} for π^-, K^- and $\bar{p}$, respectively on hydrogen, and 4.0, 3.8 and 5.0 on deuterium. The parameter b, however, was poorly determined for each cross-section measurement separately. So in the final fit it was kept fixed at the average value for a particular target, viz. $b = 5.0$ GeV/c^{-4} for hydrogen and $b = 10.0$ GeV/c^{-4} for deuterium.

The following formulae have also been tried in the extrapolating procedure

$$\sigma_i = \sigma_{tot} \exp(a\, t_i) \qquad (6)$$

$$\sigma_i = \sigma_{tot} + a\, t_i + b\, t_i^2 \qquad (7)$$

The fits obtained were statistically worse than those of equations (5) and resulted in total cross-sections about 0.5% lower than quoted. In fig. 6 are shown the curves fitted according to (5) and (6) to the partial total cross-sections for 40 GeV/c pions on hydrogen and deuterium.

For the calculation of the absorption cross-sections on complex nuclei, the partial cross-sections measured by the counters T_9 to T_{12} have been used, corresponding to $0.10 \leq |t_i| \leq 0.30$ GeV/c^2, utilizing the equation (6) for the extrapolation to $t = 0$. This procedure gave a good fit to the

data of all nuclei for all particles at all momenta. As an example the partial cross-section of 40 GeV/c π^- on all nuclei measured are displayed in Fig. 7, together with their extrapolations. The steep rise of the partial cross-section in the region $|t| \leq 0.05$ GeV/c^2, shown especially by the heavy nuclei is due to Coulomb and diffraction scattering. Their contribution is negligible for $|t| \geq 0.1$ GeV/c^2 [26].

The pion cross-sections were corrected for muon contamination in the beam. The contamination was measured directly by utilizing the high resolution Čerenkov counter $\check{C}$ with and without the coincidence signal $S\mu = S_6 S_7$ from the two counters behind the steel at the end of the beam (see fig. 8). The small correction arising from pion decay between $\check{C}$ and the centre of the targets was computed and added to the measured contamination to yield a total μ correction of 2.5 (±0.5)% at 20 GeV/c, decreasing to 1.0 (±0.4)% at 65 GeV/c (see table 4). As a check on this procedure, several cross-sections were remeasured with the signal S_6S_7 in anticoincidence with the transmission counters. The results were consistent with the data corrected as described. The kaon cross-sections have not been corrected for $K \to \mu$ decays, since this contamination produces a negligible effect on the extrapolated cross-sections. Other corrections (Coulomb, Coulomb-nuclear interference, and the effects of decays after the targets) are negligible at these energies in the t-range used.

6. Results on Elementary Cross-Sections

The measured π^-, K^- and $\bar{p}$ total cross-sections on hydrogen and deuterium are presented in Table 5 and Fig. 9. The errors quoted on each cross-section are composed of a purely statistical part, an extrapolation error and point to point uncertainties in the muon correction. Not included is a scale error originating mainly from the uncertainties in the gas densities and in the correction for muon contamination. This error is typically ±1% for the hydrogen data and ±1.2% for the deuterium data, as is indicated at the foot of the table.

Fig. 9 shows the results of this experiment together with previous measurements[3,4,5]. In general the agreement of our lower energy data with earlier results is good with the exception perhaps of the π^-p and π^-d cross-sections of Galbraith et al.[3]. In the left column of fig. 9 are shown the total cross-sections on hydrogen. Beyond 30 GeV/c the π^-p total cross-sections have become rather energy-independent within the error of about ±0.2 mb on each point, averaging about 24.6 ± 0.3 mb (this error includes the scale error). Similarly, the K^-p cross-section appears to be energy-independent, averaging 20.9 ± 0.3 mb. Only the antiproton cross-section continues to decrease, reaching a value of about 44 mb at 50 GeV/c. This value is ~ 10 to 15% larger than the estimated proton-proton total cross-section at this momentum. The behaviour of the pp and K^+p total cross-sections, as presently known, are shown by solid lines in the figure. It appears that both the K^-p and K^+p total cross-sections have become constant but at quite different values.

The middle column of Fig. 9 shows the total cross-sections on deuterium. Qualitatively the behaviour is very similar to that of the hydrogen cross-sections.

From the total cross-sections on deuterium and hydrogen the total cross-sections on neutrons have been derived, using the Glauber formula[27] to take into account the shadow effect, neglecting the Fermi motion

$$\sigma_n = \sigma_d - \sigma_p + \delta , \qquad (8)$$

where the shadow term δ is given by

$$\delta \simeq \frac{\langle r^{-2} \rangle}{4\pi} \sigma_p \sigma_n . \qquad (9)$$

The real parts of the forward scattering amplitude have been neglected in Eq. (3) since they are expected to be small. The more correct form of this equation due to Wilkin[28] gives the same results at these high-energies where charge exchange scattering is negligible. $\langle r^{-2} \rangle$ is the mean inverse square separation between the proton and the neutron in the deuteron. It is assumed that $\langle r^{-2} \rangle$ is a constant, independent of the nature of the incident particle or of its momentum, so that it can be taken from lower energy experiments. For $\langle r^{-2} \rangle$, values as low as 0.02 mb^{-1} [29,30] and as high as 0.042 mb^{-1} [3] have been derived and used in the literature, but recently a convergence towards 0.030 mb^{-1} has developed [2, 31, 32]. Such a value is in agreement with Hulthèn wave function calculations[27]. In the present work a value 0.030 mb^{-1} has therefore been adopted and, somewhat arbitrarily, an error of $\pm$0.005 mb^{-1} has been assigned to it.

Table 5 includes the computed neutron cross-sections, which are also shown in Fig. 9 (right column). Errors given represent the propagation of the errors on the proton and deuterium data. The scale error for the neutron data contains the scale errors of the constituent proton and deuterium data, assumed uncorrelated except for the uncertainty in the muon contamination, and the extra uncertainty of the Glauber correction resulting in the errors quoted at the foot of the table.

The π^-n and the K^-n cross-sections seem also to have approached energy-independent values, namely 23.3 ± 0.6 mb and 19.9 ± 0.5 mb, respectively (where the scale error is included). The difference between the cross-sections in the 35 GeV/c to 65 GeV/c region is as follows:

$$\sigma_{tot}\ (\pi^-p) - \sigma_{tot}\ (\pi^-n) = 1.3 \pm 0.7 \text{ mb}$$

$$\sigma_{tot}\ (K^-p) - \sigma_{tot}\ (K^-n) = 1.0 \pm 0.6 \text{ mb}$$

The $\bar{p}p$ and the $\bar{p}n$ cross-sections are identical within errors over the whole momentum range covered by this experiment.

From the measured hydrogen cross-sections and the computed neutron cross-sections one obtains immediately the pure isospin cross-sections. For the pion-nucleon system

$$\begin{aligned} \sigma_{3/2} &= \sigma(\pi^+p) = \sigma(\pi^-n) \\ 2\sigma_{1/2} &= 3\sigma(\pi^-p) - \sigma(\pi^+p) \end{aligned} \qquad (10)$$

For the K^--nucleon system

$$\begin{aligned} \sigma_1 &= \sigma(K^-n) \\ \sigma_0 &= 2\sigma(K^-p) - \sigma(K^-n) \end{aligned} \qquad (11)$$

For the $\bar{p}N$ system the formulae are analogous to (11).

The cross-sections of definite isotopic spin are shown in Fig. 10 and tabulated in Table 6. The errors indicated are obtained by propagating the errors on the constituent cross-sections given in Table 5. Above 30 GeV/c the $I = {}^1/_2$ πN and $I = 0$ K^-N cross-sections are approximately constant and average about 25.2 ± 0.6 mb and 22.0 ± 1.0 mb, respectively. The differences between pure isotopic spin cross-sections are

$$\sigma_{1/2}\ (\pi N) - \sigma_{3/2}\ (\pi N) = 2.0 \pm 1.0 \text{ mb}$$

$$\sigma_0\ (K^-N) - \sigma_1\ (K^-N) = 2.0 \pm 1.2 \text{ mb}$$

7. Discussion of the Elementary Hadron Cross-Sections.

The results of this experiment suggest that the total cross-sections for π^-p, π^-n, K^-p and K^-n have all become energy-independent, within the statistical errors, in the region above 30 GeV/c, whereas the $\bar{p}p$ and $\bar{p}n$ cross-sections are still decreasing.

Above 30 GeV/c the cross-sections of the two pure isospin states in the πN system and the K^-N system are on the average different by 2.0 ± 1.0 mb and 2.0 ± 1.2 mb, respectively. The errors quoted are mainly of systematic origin (gas density, Glauber correction, etc.). According to the Okun'-Pomeranchuk rule[13] the total cross-sections for particles belonging to the same isospin multiplet should asymptotically become equal because the charge exchange cross-section is assumed to vanish asymptotically. Considering the momentum range covered and the accuracy of the experiment, it seems that the present data do not contradict this rule, although the pion cross-sections appear to approach each other rather slowly (fig. 10).

For a direct comparison of the π^-n and π^+p cross-sections only the weaker assumption of charge symmetry is needed. The data in the upper graph of the right hand column of fig. 9 shows that there is good agreement between the present π^-n cross-section and previous π^+p measurements in the 20 GeV/c region.

According to the Pomeranchuk theorem[12], particle and anti-particle cross-sections must become equal in the asymptotic region. For the pion nucleon system, where particle and anti-particle belong to the same isospin multiplet, the implications of the Okun'-Pomeranchuk rule are equivalent to those of the Pomeranchuk theorem. In the case of the strange mesons, there exists an appreciable difference of 3.7 ± 0.5 mb between the newly measured K^-p cross-sections and the extrapolated value of the previously measured K^+p cross-sections in the 10 to 20 GeV/c region[3], where the data seem to be already energy-independent. If energy independence of total cross-sections is interpreted as indicating the onset of the asymptotic region, then there exists a contradiction with the Pomeranchuk theorem. In order to avoid such a contradiction one must assume that in reality some weak energy dependence persists; either the K^-p cross-section has a very slow decrease with energy, not excluded by the present data or the K^+p cross-section must increase with energy, or both. In both these cases the onset of the asymptotic region is still a long way off.

There exists a wide range of theoretical predictions regarding the high-energy behaviour of total cross-sections, usually in the framework of Regge-pole theory. The more conventional models[6] predict cross-sections that decrease towards a finite non-zero asymptotic limit. Other models[7,8] predict vanishing total cross-sections at infinity. Still others[9,10,11] predict total cross-sections rising logarithmically towards their asymptotic values. Fig. 11 shows the comparison of our data with the conventional Regge-pole fit of Barger, Olsson and Reeder[6] to previously existing data. There is a difference between the apparent energy independence of the new $\pi^- p$ and $K^- p$ data and the prediction of the model. The models that predict vanishing total cross-sections predict an even steeper fall-off with energy. The data might be in agreement with a model predicting slowly rising cross-sections, although the present data do not establish such a trend.

It has been customary to fit the high energy cross-section to simple empirical formulae of the type

$$\sigma\,(p_{lab}) = \sigma_\infty + \frac{C}{(p_{lab})^n} \qquad (12)$$

$$\sigma\,(p_{lab}) = a\, p_{lab}^{b} \qquad (13)$$

Fig. 12 shows the fit to all available total cross-section data[33,34] above 5 GeV/c to equ.(12) with n = 1 and the results of these fits are given in Table 7. Only the statistical errors have been taken into account in this procedure. The large χ^2 values in Table 7 reflects the omission of the systematic errors. Taking into account of the systematic errors in a simple way lowers the χ^2 values appreciably, without substantially changing the parameters. A value $n=\frac{1}{2}$ in equ. (12) also gives a good fit but the asymptotic cross-sections σ_∞ are different. The fit of all available data to eq.13 gives instead a considerably worse χ^2.

These facts suggest that simple dependences indicate that the data are in better agreement with finite non-zero asymptotic cross-sections. No further conclusions can be reached from this approach.

The simple quark model with SU_3 symmetry predicts[35] that the asymptotic πN and KN total cross-sections are $^2/_3$ of the asymptotic NN cross-section. Average asymptotic cross-sections obtained from Table 7 yield values of 0.6 and 0.5 for $\pi N/NN$ and KN/NN, respectively. These values may be explained by simple breaking of SU_3[6,14]. For instance, Regge-pole fits of Barger, Olsson and Reeder predict a ratio of 0.59 for $^{\pi N}/_{NN}$ and 0.50 for $^{KN}/_{NN}$, for the asymptotic cross-sections.

From the large difference in the K^-p and K^+p total cross-sections and from the approximate validity of isotopic spin invariance, it follows that the K^o regeneration amplitude must remain appreciable in the energy range above 20 GeV/c.

After the presentation of the preliminary data of this experiment several papers have appeared where these results are discussed. Barger and Philips[36], and Lendel and Ter-Martirosian[37] are able to fit the new results within the framework of a Regge pole model by adding Regge cuts. They predict total cross-sections that will rise slowly towards finite asymptotic values. Volkov, Logunov and Mestvirisvili[38], Martin[39], Eden[40] and Horn[41] discuss the possibility of the non-validity of the Pomeranchuk theorem, due to the failure of one of the assumptions on which it is based. They stress that asymptotically the real parts of the scattering amplitude might not become small.

8. Nuclear Cross-Sections

Table 8 shows the absorption cross-sections on eight nuclei for incident π^-, K^- and $\bar{p}$ at various incoming momenta.

It is not quite clear that the extrapolation procedure used for nuclei (see section 4) is applicable to a nucleus as light as Helium, because the diffraction pattern might extend still somewhat into the t-range used for extrapolation. The uncertainties on the Helium cross-sections are consequently larger.

The results displayed in Table 8 show that the momentum dependence of the absorption cross-sections for π^- and K^- is small.

The 40 GeV/c data are plotted as a function of atomic number A in Fig. 13. For each incoming particle the nuclear cross-sections lie on a straight line in a log-log plot, that is the cross-sections behave as

$$\sigma = \sigma_o A^{\alpha} \qquad (14)$$

where α, the slope of the line, seems to vary with the type of incoming particle: α increases for particles with decreasing elementary cross section, as indicated in Table 9, where the results of fitting the absorption cross-sections to eq. (14) are given. The Helium cross-sections have not been included in this fit. For a completely absorbing nucleus (black disc), one would expect $\alpha = {}^2/_3$ and for a completely transparent nucleus $\alpha = 1.0$. The values of Table 9 indicate that the $\bar{p}$ - nuclear cross-sections have a value of α close to ${}^2/_3$ while for the other particles α is larger. In a simple picture this means that the light nuclei are not completely black for incident mesons, but are essentially opaque to incident anti-protons.

Abul-Magd et al[42]) have had considerable success in describing these cross-sections by a diffraction model. No free parameters were necessary in their analysis.

Acknowledgements

We gratefully acknowledge the cooperation of many people who ensured the successful operation of the accelerator and of the secondary beam channel, and the support of Professors A.A. Logunov, R.M. Sulyaev and A.A. Naumov. We would like to express our thanks to Drs. S.S. Gerstein, L.B. Okun', K. Schlupmann, K.A. Ter-Martirosian and A.M. Wetherell for many discussions on the results of this experiment. The CERN part of the group would like to express their thanks to the directorate of IHEP for their hospitality.

TABLE 1

Scope of the measurements.

Cross-section measured	Target	Incident Particle	Range of Momentum [GeV/c]	Momentum interval between experimental points [GeV/c]
σ_{tot}	H_2, D_2	π^-	20 - 65	5
		K^-	20 - 55	5
		$\bar{p}$	20 - 50	5
σ_{abs}	He, Li, Be, C, Al, Cu Sn, Pb, U	π^-	20 - 60	10
		K^-	20 - 40	10
		$\bar{p}$	20 - 40	10

TABLE 2

The nuclear targets for which absorption cross-sections were measured.

Target	Thickness (gm cm^{-2})
Li	20.72
Be	18.57
C	34.24
Al	23.16
Cu	17.95
Sn	11.67
Pb	13.30
U	6.01

TABLE 3

Dimensions of the transmission counters.

Counter Number	Diameter (cm)	Thickness (cm)
1	6	1
2	8	1
3	10	1
4	12	1
5	14	1
6	16	1
7	18	1
8	20	1
9	24	1
10	28	2
11	34	2
12	40	2

TABLE 4

The values of the muon contamination in the beam, used in correction of the pion cross-sections. The values at 20, 25, 30, 40 and 50 GeV/c have been measured, the other were derived by interpolation and extrapolation.

Laboratory Momentum (GeV/c)	Muon Contamination %
20	2.5 ± 0.5
25	2.2 ± 0.5
30	2.0 ± 0.5
35	1.8 ± 0.5
40	1.6 ± 0.4
45	1.4 ± 0.4
50	1.3 ± 0.4
55	1.2 ± 0.4
60	1.1 ± 0.4
65	1.0 ± 0.4

Table 5

Results of the total cross-section measurements. The point to point errors are given in the table, the additional scale errors are given at the bottom of the table.

Laboratory Momentum [GeV/c]	Total cross-sections [mb]								
	$\pi^- p$	$K^- p$	$\bar{p}p$	$\pi^- d$	$K^- d$	$\bar{p}d$	$\pi^- n$	$K^- n$	$\bar{p}n$
20	25.38 ± 0.30	21.2 ± 0.6	49.0 ± 1.1	47.28 ±0.60	39.3 ± 0.6	89.5 ± 1.3	23.3 ± 0.6	19.1 ± 0.8	46.0 ± 1.7
25	24.85 ± 0.25	20.7 ± 0.4	46.1 ± 0.6	47.14 ±0.50	39.4 ± 0.5	86.5 ± 0.9	23.7 ± 0.5	19.7 ± 0.6	45.3 ± 1.1
30	24.97 ± 0.15	21.3 ± 0.3	47.1 ± 0.6	47.17 ±0.30	40.4 ± 0.4	87.0 ± 0.9	23.6 ± 0.3	20.1 ± 0.5	44.9 ± 1.1
35	24.75 ± 0.15	20.8 ± 0.3	45.5 ± 0.7	46.85 ±0.30	39.8 ± 0.4	86.4 ± 1.0	23.5 ± 0.3	19.9 ± 0.5	45.9 ± 1.2
40	24.70 ± 0.15	20.9 ± 0.3	45.0 ± 0.7	46.40 ±0.30	39.3 ± 0.4	83.5 ± 0.9	23.1 ± 0.3	19.4 ± 0.5	43.2 ± 1.1
45	24.27 ± 0.15	20.6 ± 0.3	44.9 ± 0.7	46.20 ±0.30	39.9 ± 0.4	84.8 ± 0.9	23.3 ± 0.3	20.2 ± 0.5	44.6 ± 1.1
50	24.62 ± 0.15	21.0 ± 0.4	43.6 ± 0.8	46.63 ±0.30	39.9 ± 0.5	83.1 ± 0.9	23.4 ± 0.3	19.9 ± 0.6	44.1 ± 1.2
55	24.64 ± 0.15	21.5 ± 0.6		46.44 ±0.30	40.9 ± 0.8		23.2 ± 0.3	20.4 ± 1.0	
60	24.60 ± 0.15			46.62 ±0.30			23.4 ± 0.3		
65	24.69 ± 0.20			46.76 ±0.30			23.4 ± 0.3		
Adtl.scale error	±1%	± 1%	±1%	± 1.2%	± 1.2%	± 1.2%	±2.5%	± 2.5%	± 3%

Table 6

The total cross-sections for definite isotopic spins. The point to point errors are given in the table, the additional scale errors are given at the bottom of the table.

Laboratory Momentum GeV/c	πN		$K^- N$		$\bar{p}N$	
	$I = {}^1/_2$	$I = {}^3/_2$	$I = 0$	$I = 1$	$I = 0$	$I = 1$
20	26.4 ± 0.6	23.3 ± 0.6	23.4 ± 1.5	19.1 ± 0.8	52.0 ± 2.8	46.0 ± 1.7
25	25.4 ± 0.5	23.7 ± 0.5	21.8 ± 1.0	19.7 ± 0.6	47.0 ± 1.7	45.3 ± 1.1
30	25.7 ± 0.3	23.6 ± 0.3	22.5 ± 0.8	20.1 ± 0.5	49.3 ± 1.7	44.9 ± 1.1
35	25.4 ± 0.3	23.5 ± 0.3	21.7 ± 0.8	19.9 ± 0.5	45.2 ± 1.9	45.9 ± 1.2
40	25.5 ± 0.3	23.1 ± 0.3	22.4 ± 0.8	19.4 ± 0.5	46.8 ± 1.8	43.2 ± 1.1
45	24.8 ± 0.3	23.3 ± 0.3	21.0 ± 0.8	20.2 ± 0.5	45.3 ± 1.8	44.6 ± 1.1
50	25.2 ± 0.3	23.4 ± 0.3	22.1 ± 1.0	19.9 ± 0.6	43.0 ± 2.0	44.1 ± 1.2
55	25.4 ± 0.3	23.2 ± 0.3	22.7 ± 1.6	20.4 ± 1.0		
60	25.2 ± 0.3	23.4 ± 0.3				
65	25.3 ± 0.4	23.4 ± 0.3				
Additional scale error	± 2%	± 2.5%	± 3.4%	± 2.5%	± 3.5%	± 3.0%

TABLE 7

Results of the least square fits to all the published total cross-sections above 5 GeV/c laboratory momentum to the equ. (12) with n = 1. Only the statistical errors on each oint have been taken into consideration.

Total cross-section	Number of points	σ_∞ (mb)	C	χ^2
$\pi^- p$	84	23.99 ± 0.02	26.41 ± 0.13	161
$\pi^+ p = \pi^- n$	66	22.66 ± 0.03	19.53 ± 0.17	200
$K^- p$	30	20.06 ± 0.14	25.16 ± 1.60	43
$K^- n$	18	19.49 ± 0.23	6.21 ± 2.20	-
$K^+ p$	20	17.39 ± 0.09	-1.31 ± 0.93	66
$K^+ n$	11	17.63 ± 0.29	0.55 ± 2.48	-
pp	52	38.32 ± 0.05	14.73 ± 0.32	184
pn	16	37.63 ± 0.41	24.3 ± 2.5	57
$\bar{p}p$	24	42.35 ± 0.35	111.1 ± 4.5	37
$\bar{p}n$	17	42.42 ± 0.54	87.8 ± 6.0	-

TABLE 8

Absorption cross-sections in mb per nucleus.

Mom. (GeV/c)	Part.	Nucleus and atomic numbers.								
		He 4.0	Li 6.94	Be 9.01	C 12.01	Al 26.98	Cu 63.54	Su 118.7	Pb 207.2	U 238
20	π^-	-	126 ± 2	154 ± 2	186 ± 3	349 ±7	657 ± 10	1044 ± 12	1550 ± 20	1860 ± 70
	K^-	-	110 ± 3	144 ± 5	169 ± 4	310 ±10	555 ± 20	885 ± 50	1330 ± 70	1600 ± 200
	$\bar{p}$	-	215 ± 7	240 ± 10	290 ± 15	500 ±20	965 ± 60	1300 ± 120	1810 ±150	2030 ± 320
30	π^-	73 ±3	120 ± 2	149 ± 3	177 ±2	340 ± 6	640 ± 8	1030 ± 20	1525 ± 25	1815 ± 35
	K^-	65 ±3	107 ± 2	134 ± 4	157 ±3	308 ±10	616 ± 22	933 ± 20	1385 ± 45	1615 ± 80
	$\bar{p}$	117 ±5	188 ± 4	235 ±6	258 ±6	457 ±11	890 ± 30	1210 ± 45	1880 ± 65	2020 ± 125
40	π^-	74 ±3	121 ± 2	148 ±2	179 ±2	339 ±4	640 ± 7	1040 ± 15	1510 ± 20	1710 ± 35
	K^-	65 ±3	105 ± 2	137 ±2	162 ±2	313 ±6	593 ± 10	920 ± 30	1408 ± 30	1600 ± 50
	$\bar{p}$	119 ±5	168 ± 8	226 ±7	257 ±5	490 ±15	820 ± 30	1240 ± 70	1790 ± 80	1820 ± 200
50	π^-	76 ±3	124 ± 2	149 ±2	178 ±2	338 ±4	635 ± 7	1040 ± 15	1525 ± 20	1700 ± 25
60	π^-	74 ±3	123 ± 3	151 ±3	182 ±3	340 ±4	654 ± 15	1020 ± 20	1510 ± 25	1775 ± 50

TABLE 9

Results of the least square fits of the absorption cross-sections to the formula $\sigma_{abs} = \sigma_o A^{\alpha}$.
All the nuclei except He have been fitted, giving 8 data points.

Part.	Mom. (GeV/c)	α	σ_o (mb)	χ^2
π^-	20	0.743 ± 0.003	30.0 ± 0.5	6.2
	30	0.760 ± 0.005	27.4 ± 0.7	13.4
	40	0.750 ± 0.004	28.2 ± 0.5	9.8
	50	0.748 ± 0.004	28.5 ± 0.6	12.2
	60	0.745 ± 0.004	29.1 ± 0.6	5.8
K^-	20	0.727 ± 0.007	27.7 ± 0.9	4.4
	30	0.765 ± 0.007	24.3 ± 0.7	8.3
	40	0.759 ± 0.006	25.0 ± 0.7	14.3
$\bar{p}$	20	0.648 ± 0.010	59.1 ± 2.6	4.2
	30	0.674 ± 0.009	50.9 ± 2.4	15.2
	40	0.674 ± 0.010	49.9 ± 2.4	9.5

REFERENCES

1. A. Citron, W. Galbraith, T.F. Kycia, B.A. Leontic, R.H. Phillips, A. Rousset and P.H. Sharp, Phys.Rev. 144, 1101 (1966).

2. D.V. Bugg, D.C. Salter, G.H. Stafford, R.F. George, K.F. Riley and R.J. Tapper, Phys.Rev. 146, 980 (1966).

3. W. Galbraith, E.W. Jenkins, T.F. Kycia, B.A. Leontic, R.H. Phillips, A.L. Read and R. Rubinstein, Phys.Rev. 138 B, 913 (1965).

4. G. von Dardel, D. Dekkers, R. Mermod, M. Vivargent, G. Weber and K. Winter, Phys.Rev. Letters 8, 173 (1962).

5. K.J. Foley, R.S. Jones, S.J. Lindenbaum, W.A. Love, S. Ozaki, E.D. Platner, C.A. Quarles, E.H. Willen, Phys.Rev.Letters 19, 330, 857 (1967).

6. V. Barger, M. Olsson and D.D. Reeder, Nuclear Phys. B5, 411 (1968).

7. N. Cabibbo, L. Horwitz, J.J.J. Kokkedee and Y. Néeman, Nuovo Cimento 45 A, 275 (1966).

8. H. Cheng and T.T. Wu, Phys.Rev. Letters 22, 1405 (1969).

9. S. Frautschi and B. Margolis, Nuovo Cimento 56 A, 1155 (1968) N.W. Dean, Phys.Rev. 182, 1695 (1969).

10. V.N. Gribov and A.A. Migdal, Yadernaya Fisika 8, 1213 (1968). [English translation: Soviet Journal of Nuclear Phys. 8, (1969)].

11. V.R. Garsevanishvili, V.A. Matveev, L.A. Slepchenko and A.N Tavkhelidze, JINR Preprint E2-4251 (1969).

12. I.Ia. Pomeranchuk, Zhur. Eksp. i Teoret. Fiz. 34, 725 (1958) [English Translation: Soviet Phys. - JETP 7, 499 (1958)].

13. L.B. Okun' and I.Ia. Pomeranchuk, Zhur Eksp. i Teoret.Fiz. 30, 424 (1956) [English translation: Soviet Phys. - JETP 3, 307 (1956)].

14. R.H. Dalitz, Proceedings of the 1967 International Conference on Pion-Nuclear Scattering at Irvine.
J.J.J. Kokkedee, The Quark Model (W.A. Benjamin, New York) 1969.

15. R.J. Glauber, 2nd International Conference on High Energy Physics and Nuclear Structure, Rehovoth, Israel (1967).

16. L.R.B. Elton, Nuclear Sizes (Oxford University Press) 1961.

17. H. Feshbach, International School of Physics "Enrico Fermi", Varenna, Course 38 (1966).

18. J.V. Allaby, Yu.B. Bushnin, S.P. Denisov, A.N. Diddens, R.W. Dobinson, S.V. Donskov, G. Giacomelli, Yu.P. Gorin, A. Klovning, A.I. Petrukhin, Yu.D. Prokoshkin, R.S. Shuvalov, C.A. Stahlbrandt, D.A. Stoyanova, Physics Letters 30 B, 500 (1969).

19. Yu.B. Bushnin, S.P. Denisov, S.V. Donskov, A.F. Dunaitsev, Yu.P. Gorin, V.A. Kachanov, Yu.S. Khodirev, V.I. Kotov, V.M. Kutyin, A.I. Petrukhin, Yu.D. Prokoshkin, E.A. Razuvaev, R.S. Shuvalov, D.A. Stoyanova; J.V. Allaby, F. Binon, A.N. Diddens, P. Duteil, G. Giacomelli, R. Meunier, J.P. Peigneux, K. Schlupmann, M. Spighel, C.A. Stahlbrandt, J.P. Stroot and A.M. Wetherell, Phys.Letters 29 B, 48 (1969), and Yadernaya Fisika 10, 585 (1969).

I.A. Aleksandrov, M.I. Grachev, K.I. Gubrienko, E.V. Eremenko, V.I. Kotov, A.N. Nekrasov, A.A. Prilepin, V.A. Pichugin, R.A. Rzaiev, A.V. Samojlov, V.C. Seleznev, B.A. Serebrjakov, A.E. Khanamirjan and Yu.S. Khodyrev, Preprint IHEP 69-36.

20. Yu.P. Gorin, S.P. Denisov, S.V. Donskov, A.F. Dunaitsev, A.I. Petrukhin, Yu.D. Prokoshkin, R.S. Shuvalov and D.A. Stoyanova, Preprint IHEP-69-63.

21. W.A. Rabinovich, Inzh.-Fiz. Zhur., Akad. Nauk Belorussk SSR 5, 30 (1962).

22. J. Hilsenrath, C.W. Beckett, W.S. Benedict, L. Fano, H.J. Hoge, J.F. Masi, R.L. Nuttall, Y.S. Touloukiar and H.W. Woolley, "Tables of Thermal Properties of Gases", National Bureau of Standards (Washington), Circular 564 (1955).

R.D. Goodwin, D.E. Diller, H.M. Roder and L.A. Weber, Journal of Research NBS 68 A, 121 (1964).

H.L. Johnston and D. White, Trans. Am. Soc. Mech. Eng. 72, 785 (1950).

23. A. Michels, W. de Graaff, T. Wassenaar, J.M.H. Levelt and P. Louwerse, Physics 25, 25 (1959).

24. J.A. Beattie and W.H. Stockmayer, Rep. Progr. Physics 7, 195 (1940).

25. S.V. Donskov, Yu.D. Prokoshkin and R.S. Shuvalov, Preprint IHEP-68-22, and Pribory i Tekhnika Eksperimenta 6, 18 (1969).

26. G. Bellettini, G. Cocconi, A.N. Diddens, E. Lillethun, G. Matthiae, J.P. Scanlon and A.M. Wetherell, Nuclear Physics 79, 609 (1966).

27. R.J. Glauber, Phys.Rev. 100, 242 (1955).
V. Franco and R.J. Glauber, Phys.Rev. 142, 1195 (1966).

28. C. Wilkin, Phys.Rev. Letters 17, 561 (1966).

29. W.F. Baker, E.W. Jenkins, T.F. Kycia, R.H. Phillips, A.L. Read, K.F. Riley and H. Ruderman, Proc. Int. Conf. on Elementary Particles and High-Energy Physics, Sienna (1963), Vol. I, p.634.

30. A.A. Carter, K.F. Riley, R.J. Tapper, D.V. Bugg, R.S. Gilmore, K.M. Knight, D.C. Salter, G.H. Stafford, E.J.N. Wilson, J.D. Davies, J.D. Dowell, P.M. Hattersley, R.J. Homer and A.W. O'Dell, Phys.Rev. 168, 1457 (1968).

31. R.J. Abrams, R.L. Cool, G. Giacomelli, T.F. Kycia, B.A. Leontic, K.K. Li and D.M. Michael, Phys.Rev. Letters 18, 1209 (1967).

R.L. Cool, G. Giacomelli, T.F. Kycia, B.A. Leontic, K.K. Li, A. Lundby, J. Teiger and C. Wilkin, to be published in Phys.Rev.

32. D.V. Bugg, R.S. Gilmore, K.M. Knight, D.C. Salter, G.H. Stafford, E.J. Wilson, J.D. Davies, J.D. Dowell, P.M. Hattersley, R.J. Homer, A.W. O'Dell, A.A. Carter, R.J. Tapper and K.F. Riley, Phys.Rev. 168, 1466 (1968).

33. G. Giacomelli, P. Pini and S. Stagni, Reports CERN-HERA 69-1 (1969) and 70-3 (1970).

34. W. Galbraith, Reports on Progress in Physics, 32, 547 (1969).
G. Giacomelli, Progress in Nuclear Physics, Vol. 12 (1970) (in press).

35. F.M. Levin and L.L. Frankfurt, Soviet Phys. - JETP Letters 2, 65 (1965).

H.J. Lipkin and F. Scheck, Phys.Rev. Letters 16, 71 (1966).

36. V. Barger and R.J.N. Phillips, Phys.Rev. Letters 24, 291 (1970).

37. A.N. Lendel and K.A. Ter-Martirosian, JETP Letters 11, 70 (1970).

38. G.G. Volkov, A.A. Logunov and M.A. Mestvirisvili, Preprint IHEP 69-110 (Serpukhov, 1969).

39. A. Martin, Report Th. 1075 - CERN (1969).

40. R.J. Eden, Preprint, University of California, Riverside, UCR - 34 P 107 - 105 (1969).

41. D. Horn, Phys.Lett. 31B, 30 (1970).

42. A.Y. Abul-Magd, G. Alberi and L. Bertocchi, Phys.Letters 30B, 182 (1969).

Figure Captions

Fig. 1a : Principle of the measurement. S counts the incoming beam, G is the target and T_i are the transmission counters.

Fig. 1b : Layout of the beam and of the experimental equipment. 1, 2, and 3 indicate the positions of the internal aluminium targets. K_1, K_2, and K_3 are collimators, L_1 - L_{10} are quadrupole lenses, M_1 - M_4 are bending magnets, S_1 - S_7 are scintillation counters, A_1 and A_2 are anti-coincidence scintillation counters, D and Č are the differential and the threshold Čerenkov counters, T_1 - T_{12} are the transmission counters, W is the wedge-shaped detector; H_2, D_2, He and E are the target cells. F_{1-4} and P_{1-3} are monitor telescopes. G_2 are the nuclear targets.

Fig. 2 : Pressure curve of the gas differential Cerenkov counter (DISC) at 45 GeV/c.

Fig. 3 : Schematic diagram of a gas target.

Fig. 4 : Beam profile curves, measured by the wedge - shaped detectors at the position of the transmission counters.

Fig. 5 : Block diagram of the electronics.

Fig. 6 : Example of the extrapolation procedure to zero solid angle for π^-p and π^-D total cross-section measurements at 40 GeV/c. The fit shown by solid line is the one finally adopted.

Fig. 7 : The extrapolation of the partial cross-sections to zero solid angle for 40 GeV/c π^- on nuclei to obtain the absorption cross-section. For reasons of completeness also the H_2 and D_2 partial cross-sections are shown.

Fig. 8 : Pressure curve of the high resolution threshold Čerenkov counter for a measurement of the muon contamination in the beam at 30 GeV/c. The bottom curve was obtained with the counters Sμ behind the iron block in coincidence, the top curve without.

Fig. 9 : Total cross-section on hydrogen (left column), deuterium (middle column), and neutrons (right column) for π^- (top row), K^- (middle row), and $\bar{p}$ (bottom row) particles. The scale errors are not shown (see table). The value $\langle r^{-2} \rangle = 0.03$ has been used in the Glauber-Wilkin correction. Some hand fits to positive particle total cross-sections are shown for comparison (full line).
Δ: See ref. 3; +: See ref. 4; O: See ref. 5
●: this experiment.

Fig. 10 : Pure isospin total cross-sections. Only the statistical errors are shown; for the scale error see text.

Fig. 11 : Comparison of the negative particle total-cross-sections with the Regge-pole model predictions of Barger, Olsson and Reeder (ref. 6). The scale errors are not shown (see Table).

Fig. 12 : A compilation of the high energy total cross-sections. Only the data points on hydrogen are shown. The lines are the results of the least squares fits to the total cross-sections above 5 GeV/c using eq. (12) with n = 1. Solid lines represent fits to proton data, broken lines to neutron data. Extrapolations are indicated by a dashed extension of the fitted lines.

Fig. 13 : Absorption cross-sections for 40 GeV/c π^-, K^- and $\bar{p}$ as a function of A. The lines are fits to eq. (14).

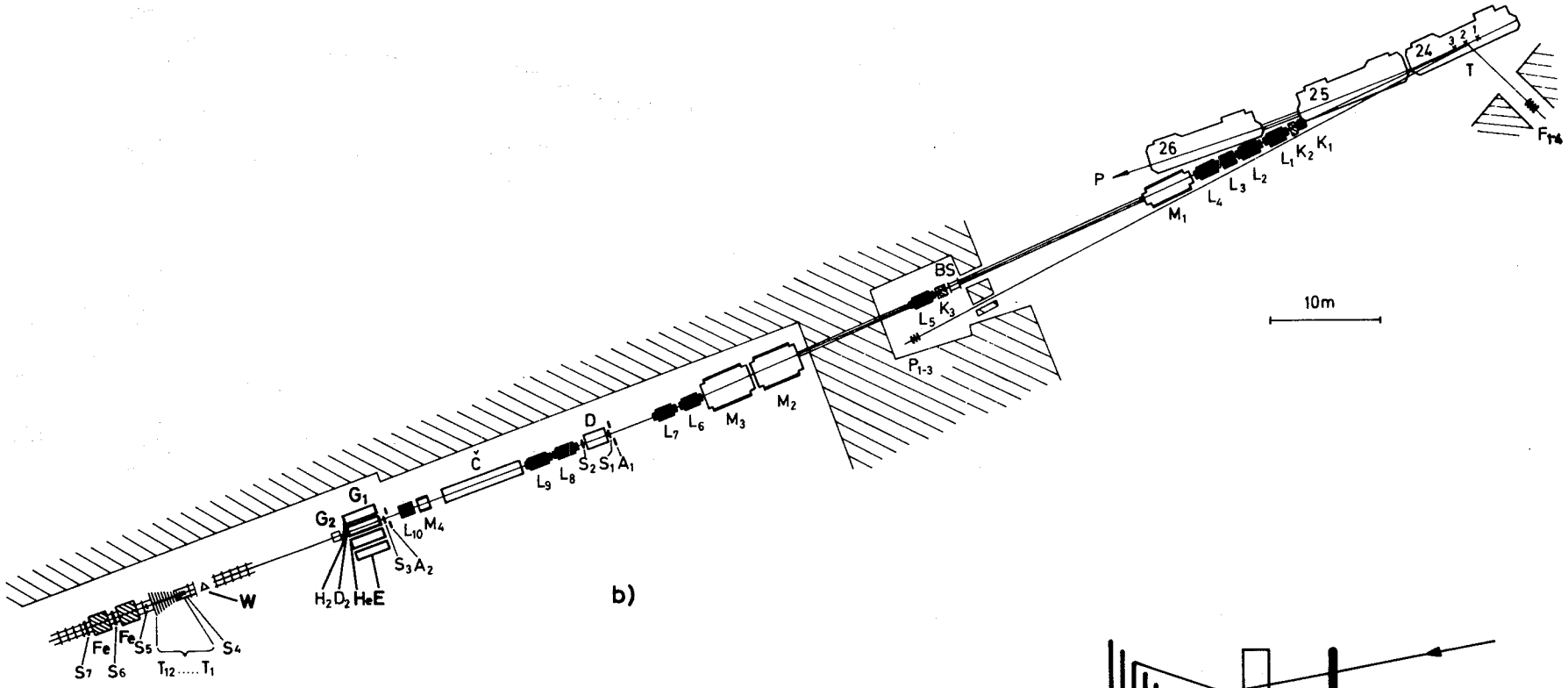
24
25
26
T
P
BS
10m
W
Fe
Fe
S7
S6
S5
S4
T12 ..... T1
H2 D2 HeE
G1
G2
S3 A2
L10 M4
Č
L9 L8
S2 S1 A1
D
L7 L6 M3
M2
P1-3
L5 K3
M1
L4 L3 L2 L1 K2 K1
b)

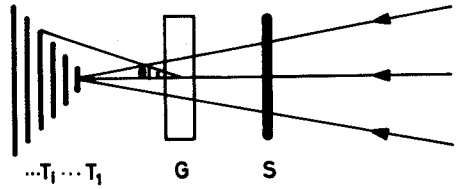
...T1 ... T1
G
S
a)

Fig:1

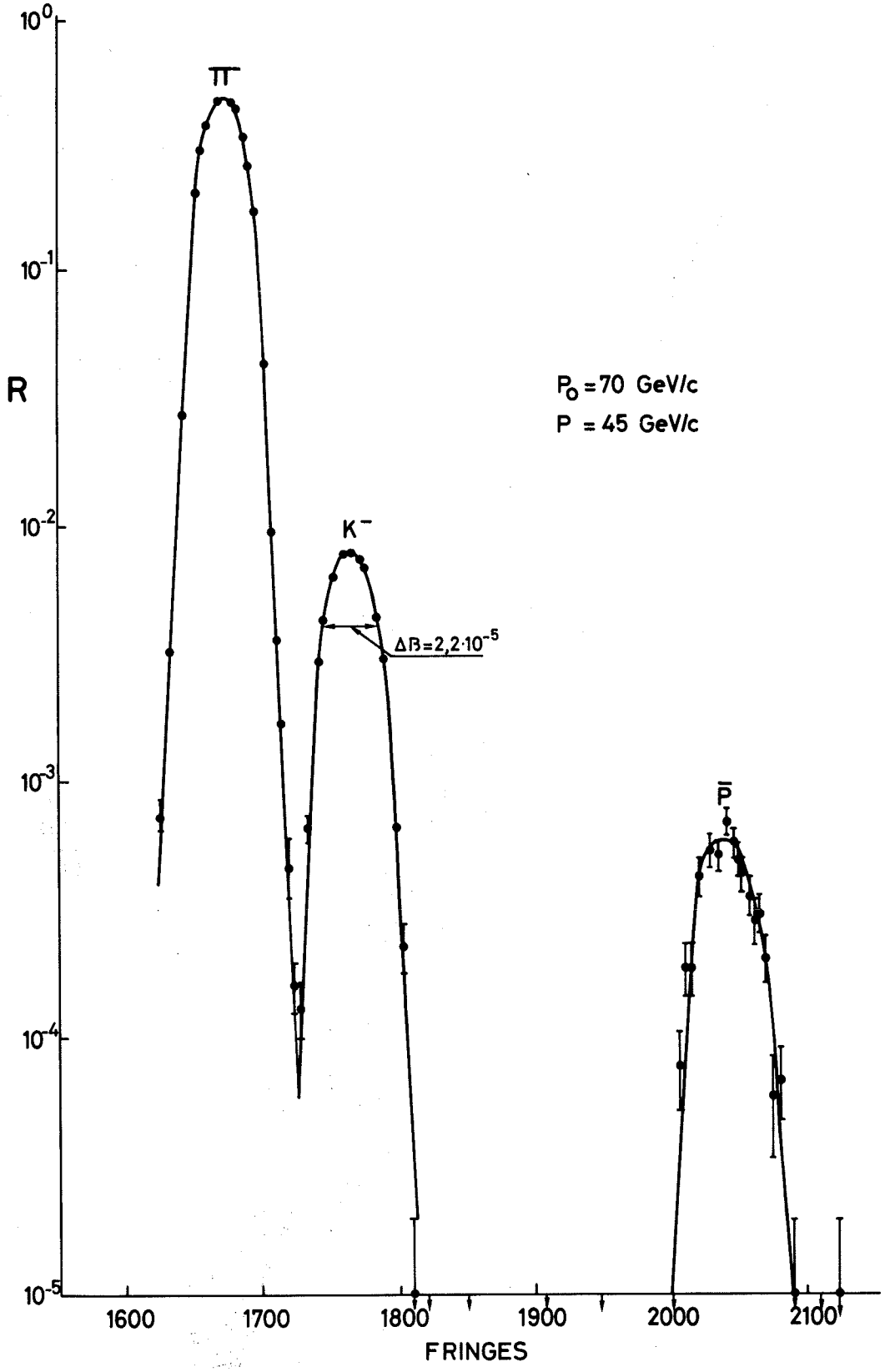
10^0
10^{-1}
10^{-2}
10^{-3}
10^{-4}
10^{-5}
R
π^-
K^-
$\bar{P}$
$\Delta B = 2,2 \cdot 10^{-5}$
$P_o = 70$ GeV/c
$P = 45$ GeV/c
1600
1700
1800
1900
2000
2100
FRINGES

Fig: 2

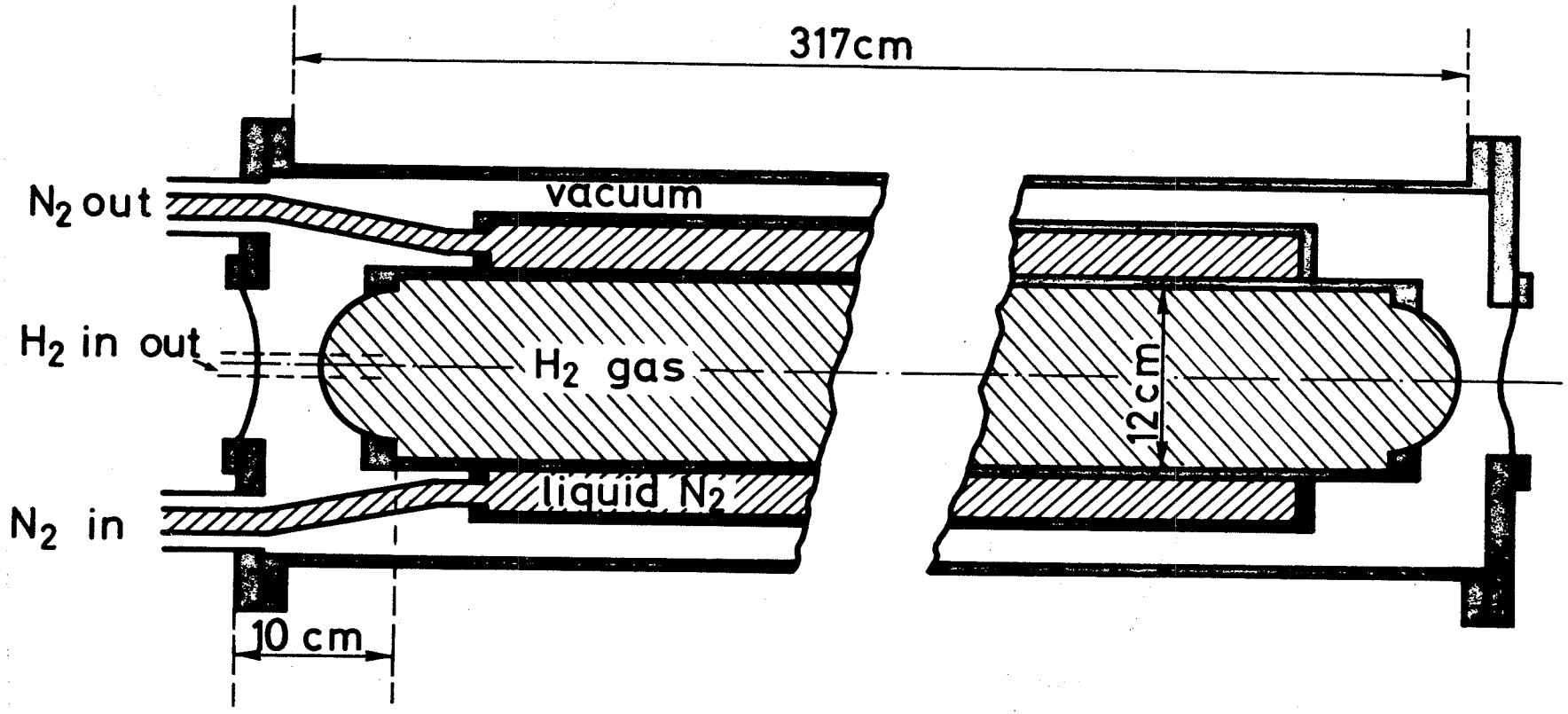

SCHEMATIC OF A GAS TARGET GEOMETRY

Fig: 3

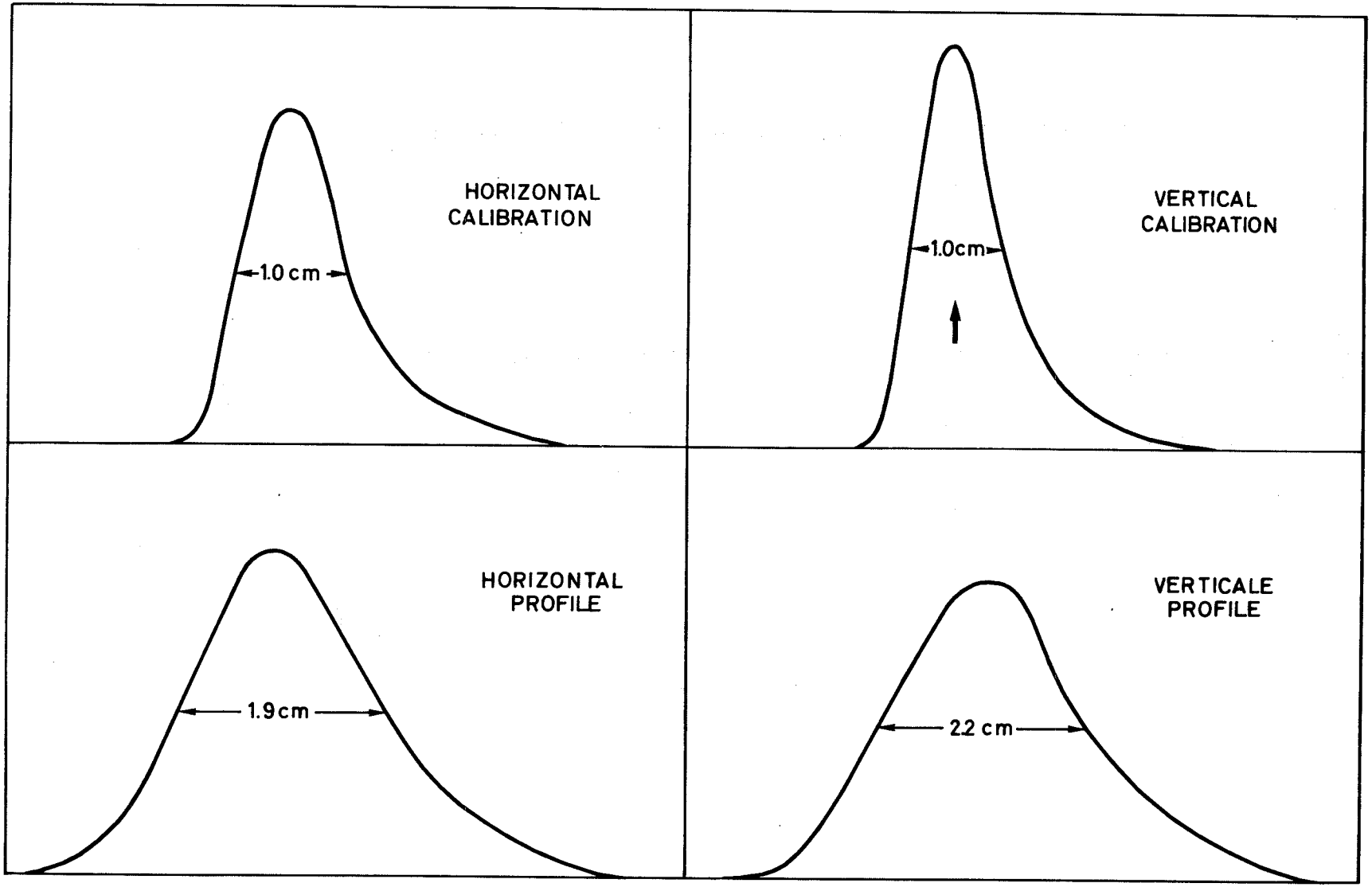
HORIZONTAL
CALIBRATION
1.0 cm
VERTICAL
CALIBRATION
1.0cm
HORIZONTAL
PROFILE
1.9cm
VERTICALE
PROFILE
2.2 cm

Fig: 4

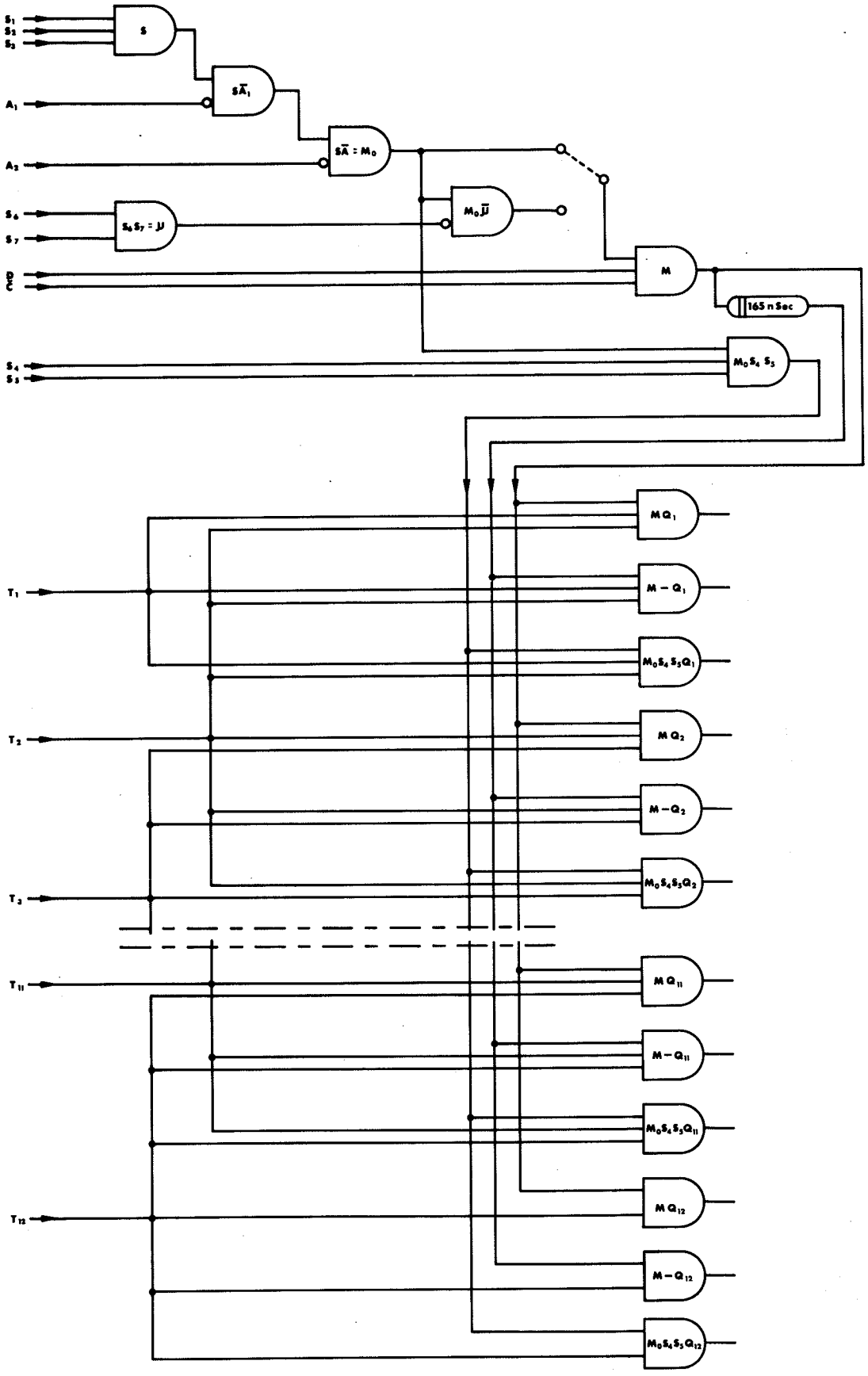
S1
S2
S3
S
A1
A2
S4
S7
S6 S7 = μ
M0 μ̄
M
165 n Sec
M0 S4 S5
S4
S5
T1
T2
T3
T11
T12
M Q1
M − Q1
M0 S4 S5 Q1
M Q2
M − Q2
M0 S4 S5 Q2
M Q11
M − Q11
M0 S4 S5 Q11
M Q12
M − Q12
M0 S4 S5 Q12

Fig:5

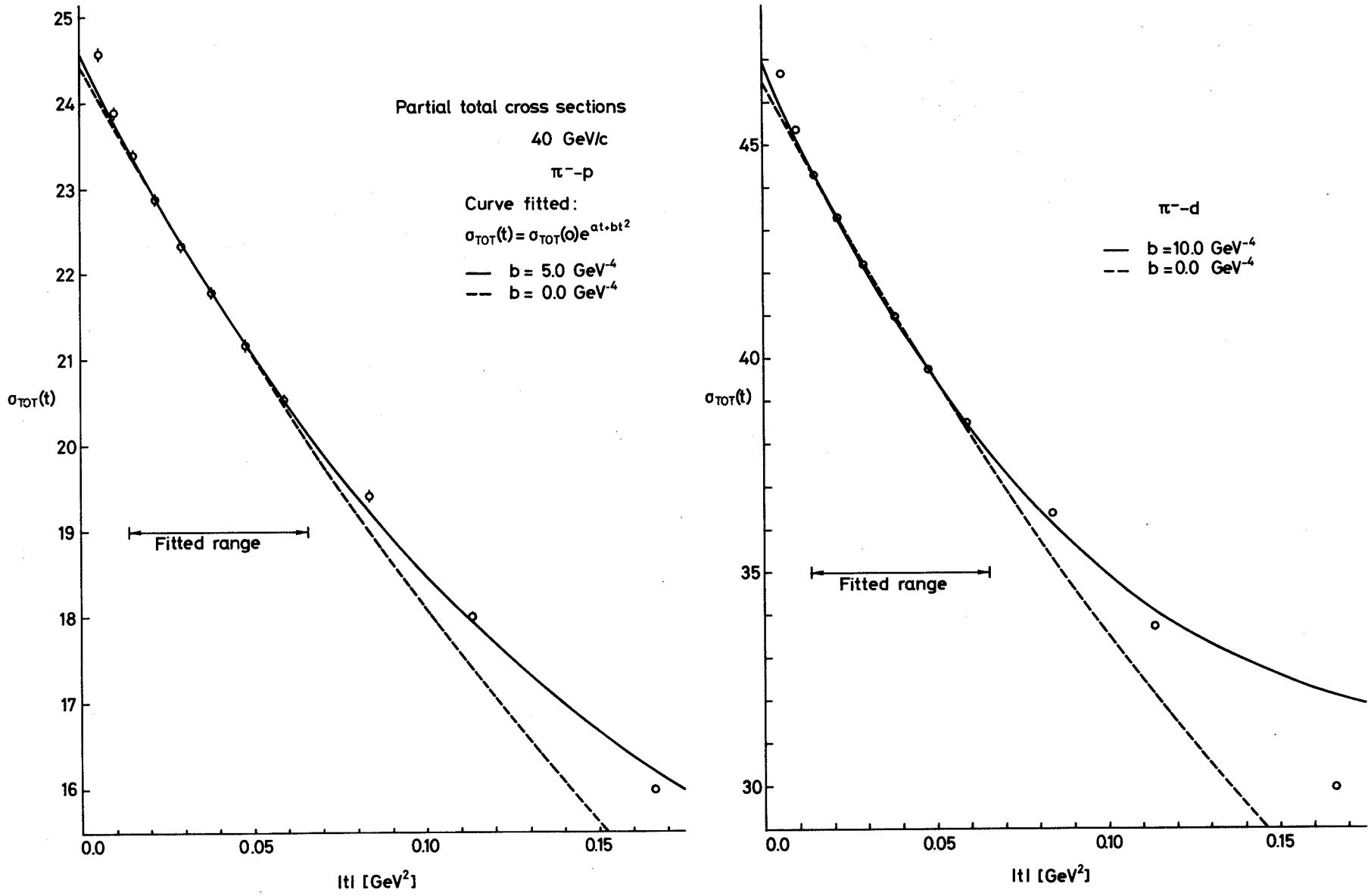
Partial total cross sections
40 GeV/c
π⁻-p
Curve fitted:
$\sigma_{TOT}(t) = \sigma_{TOT}(o)e^{at+bt^2}$
— b = 5.0 GeV⁻⁴
-- b = 0.0 GeV⁻⁴
Fitted range
$\sigma_{TOT}(t)$
|t| [GeV²]
π⁻-d
— b = 10.0 GeV⁻⁴
-- b = 0.0 GeV⁻⁴
Fitted range
$\sigma_{TOT}(t)$
|t| [GeV²]

Fig:6

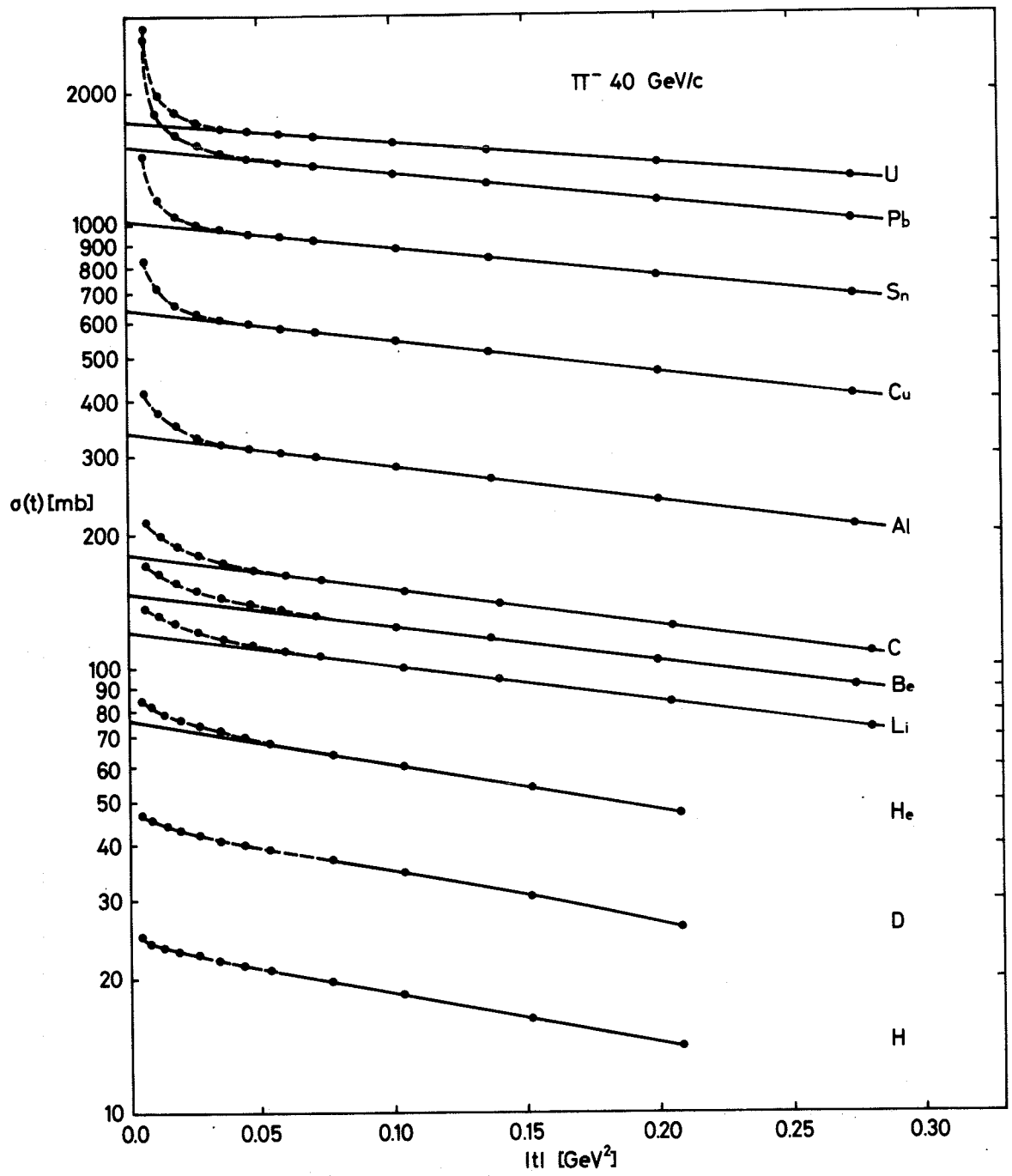
π⁻ 40 GeV/c
2000
1000
900
800
700
600
500
400
300
200
100
90
80
70
60
50
40
30
20
10
σ(t) [mb]
U
Pb
Sn
Cu
Al
C
Be
Li
He
D
H
0.0
0.05
0.10
0.15
0.20
0.25
0.30
|t| [GeV²]

Fig:7

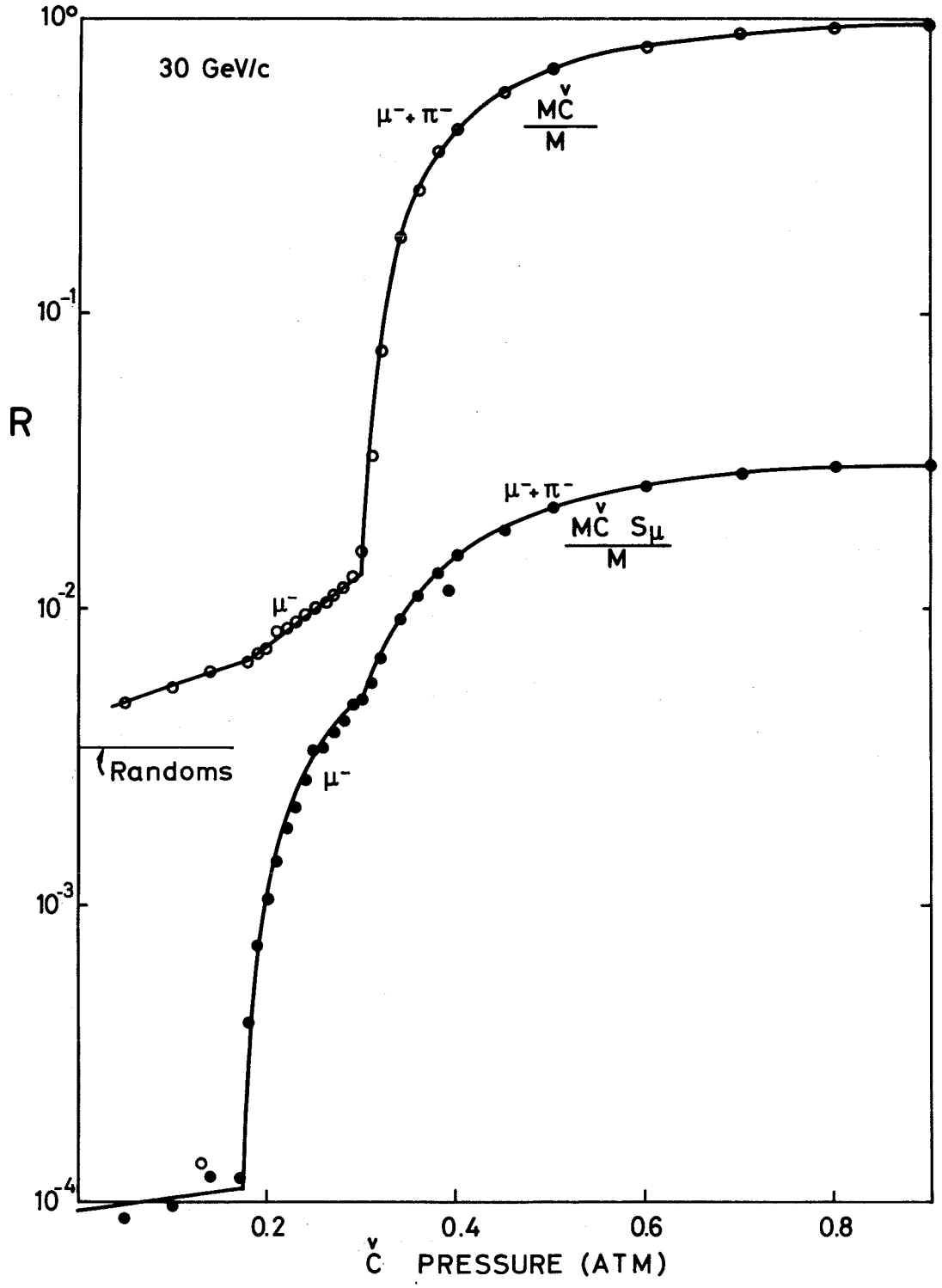
10°
30 GeV/c
μ⁻+π⁻
MC/M
10⁻¹
R
μ⁻+π⁻
MC Sμ/M
10⁻²
μ⁻
Randoms
μ⁻
10⁻³
10⁻⁴
0.2
0.4
0.6
0.8
C PRESSURE (ATM)

Fig:8

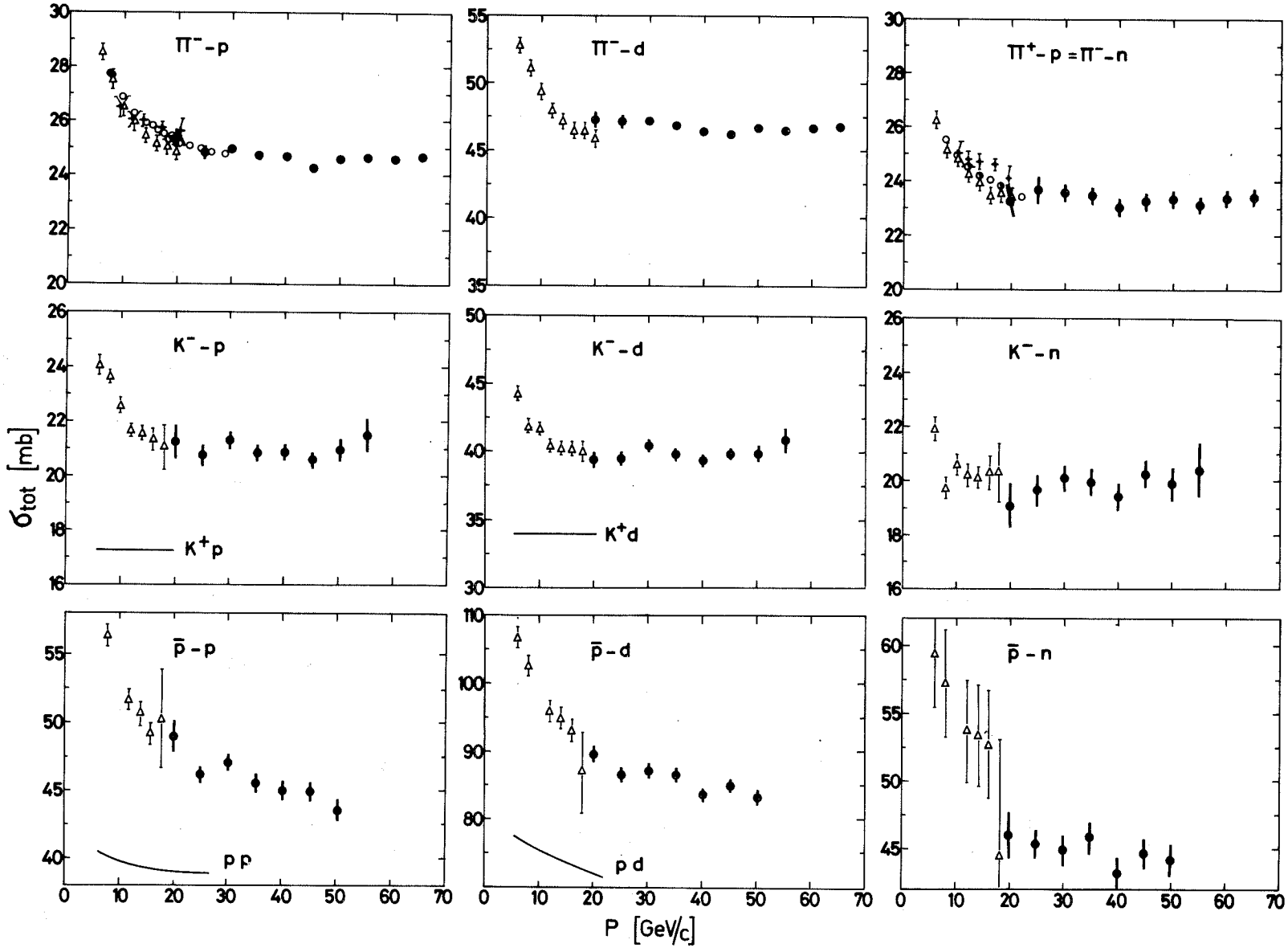

Fig:9

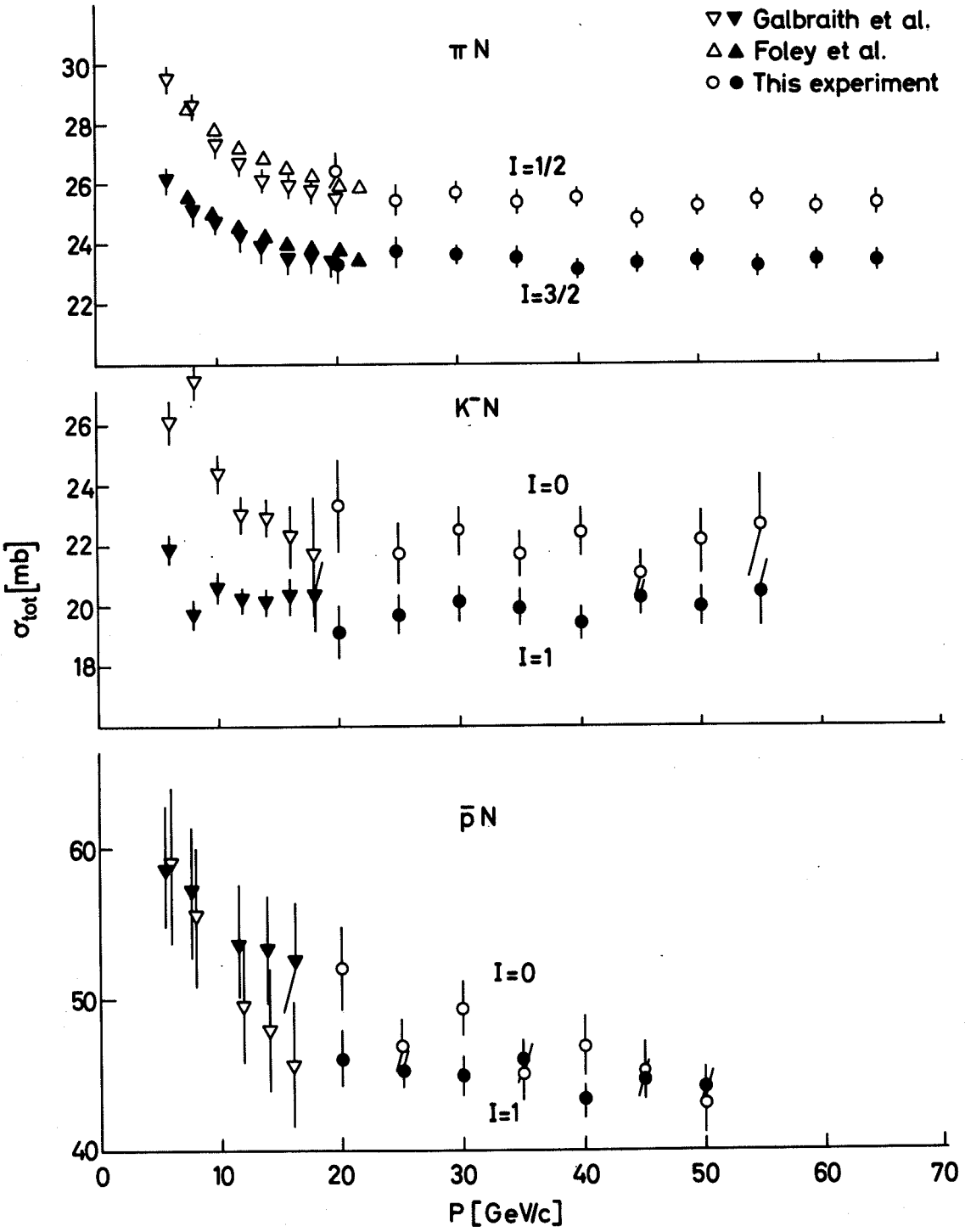
▽▼ Galbraith et al.
△▲ Foley et al.
○ ● This experiment
π N
I=1/2
I=3/2
K⁻N
I=0
I=1
p̄N
I=0
I=1
σtot [mb]
P [GeV/c]

Fig:10

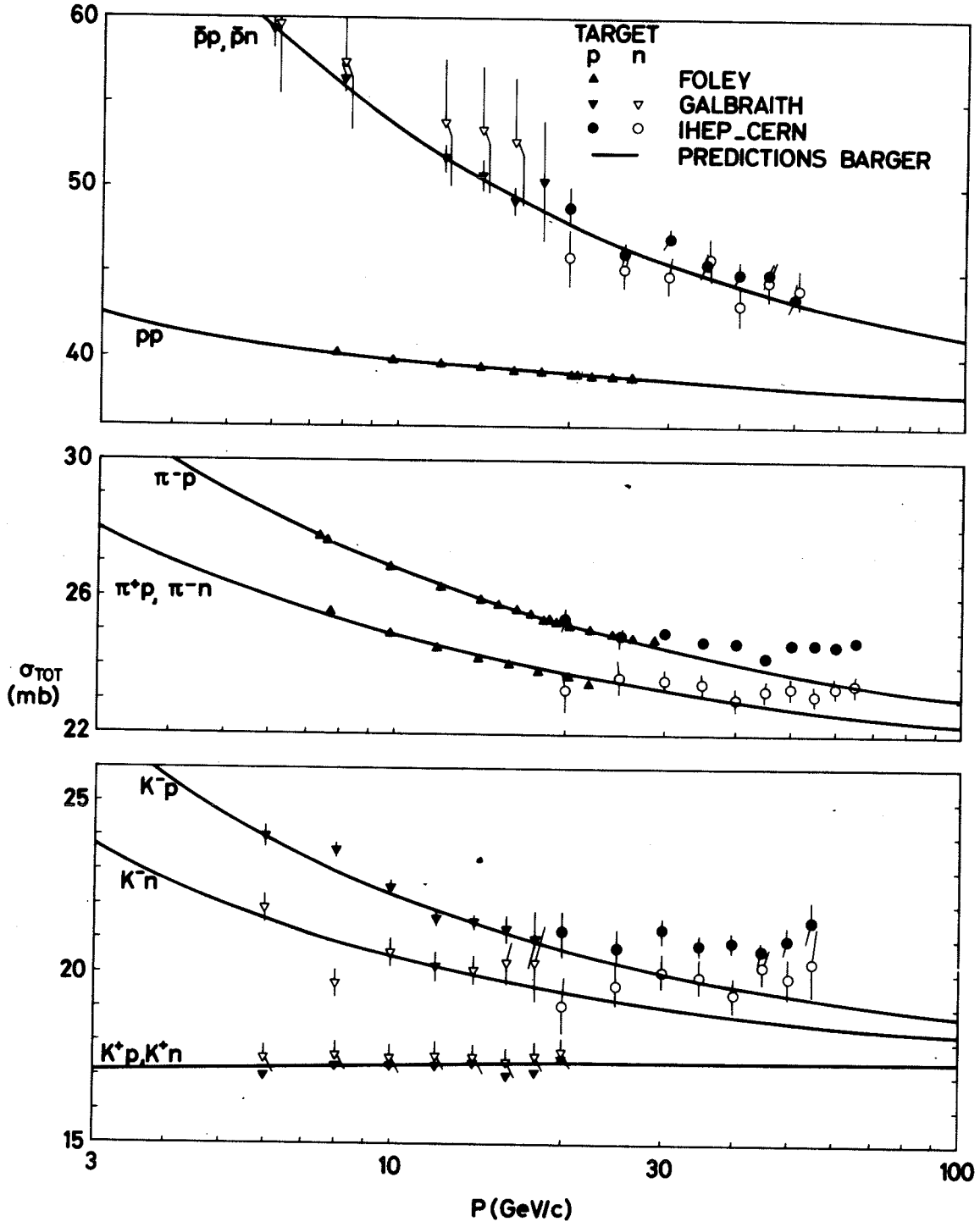
60
50
40
30
26
22
25
20
15
3
10
30
100
$\bar{p}p, \bar{p}n$
pp
π^-p
π^+p, π^-n
K^-p
K^-n
K^+p, K^+n
TARGET
p n
FOLEY
GALBRAITH
IHEP_CERN
PREDICTIONS BARGER
σ_{TOT} (mb)
P (GeV/c)

Fig :11

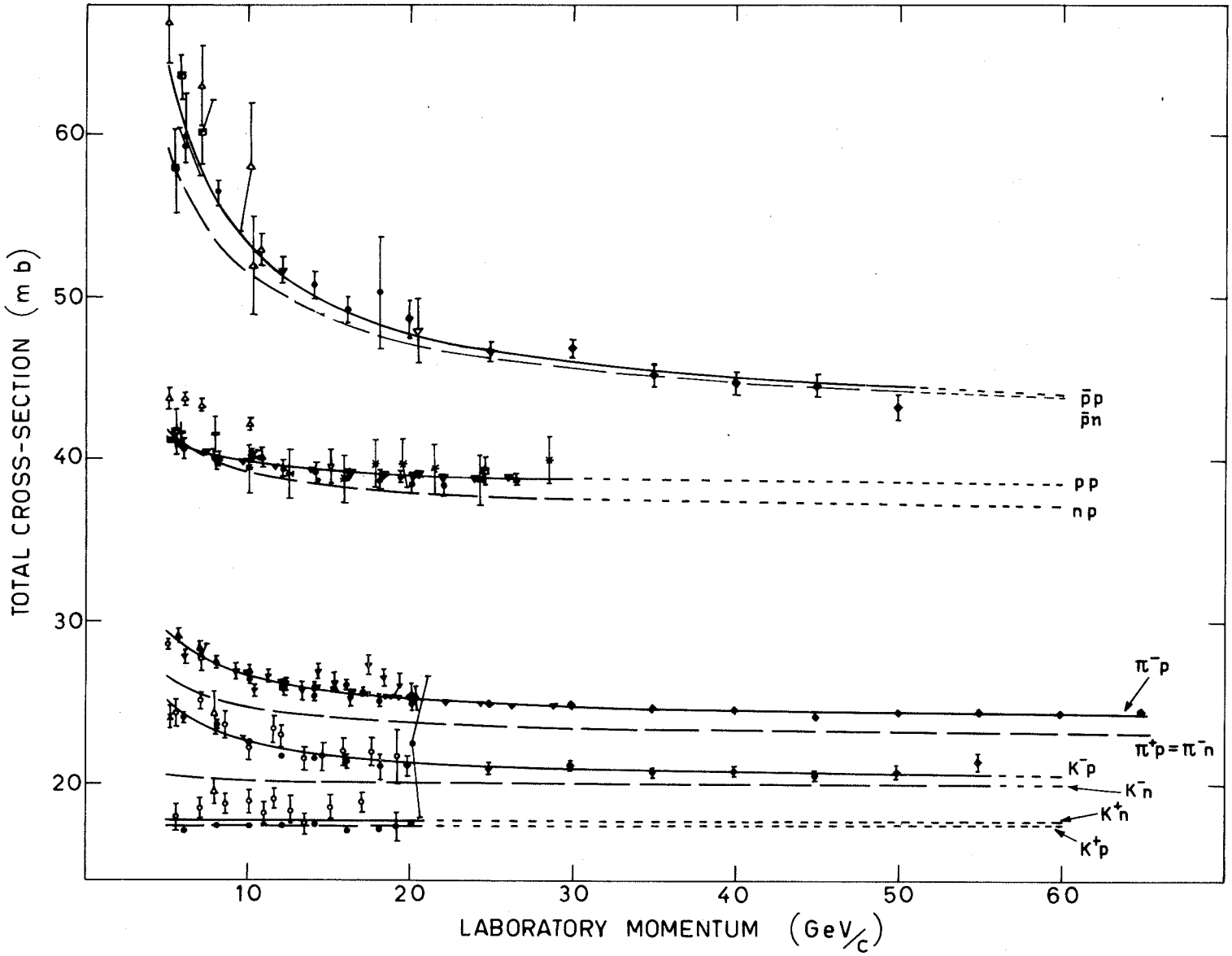
TOTAL CROSS-SECTION (m b)
60
50
40
30
20
10
20
30
40
50
60
LABORATORY MOMENTUM (GeV/c)
p̄p
p̄n
pp
np
π⁻p
π⁺p=π⁻n
K⁻p
K⁻n
K⁺n
K⁺p

Fig:12

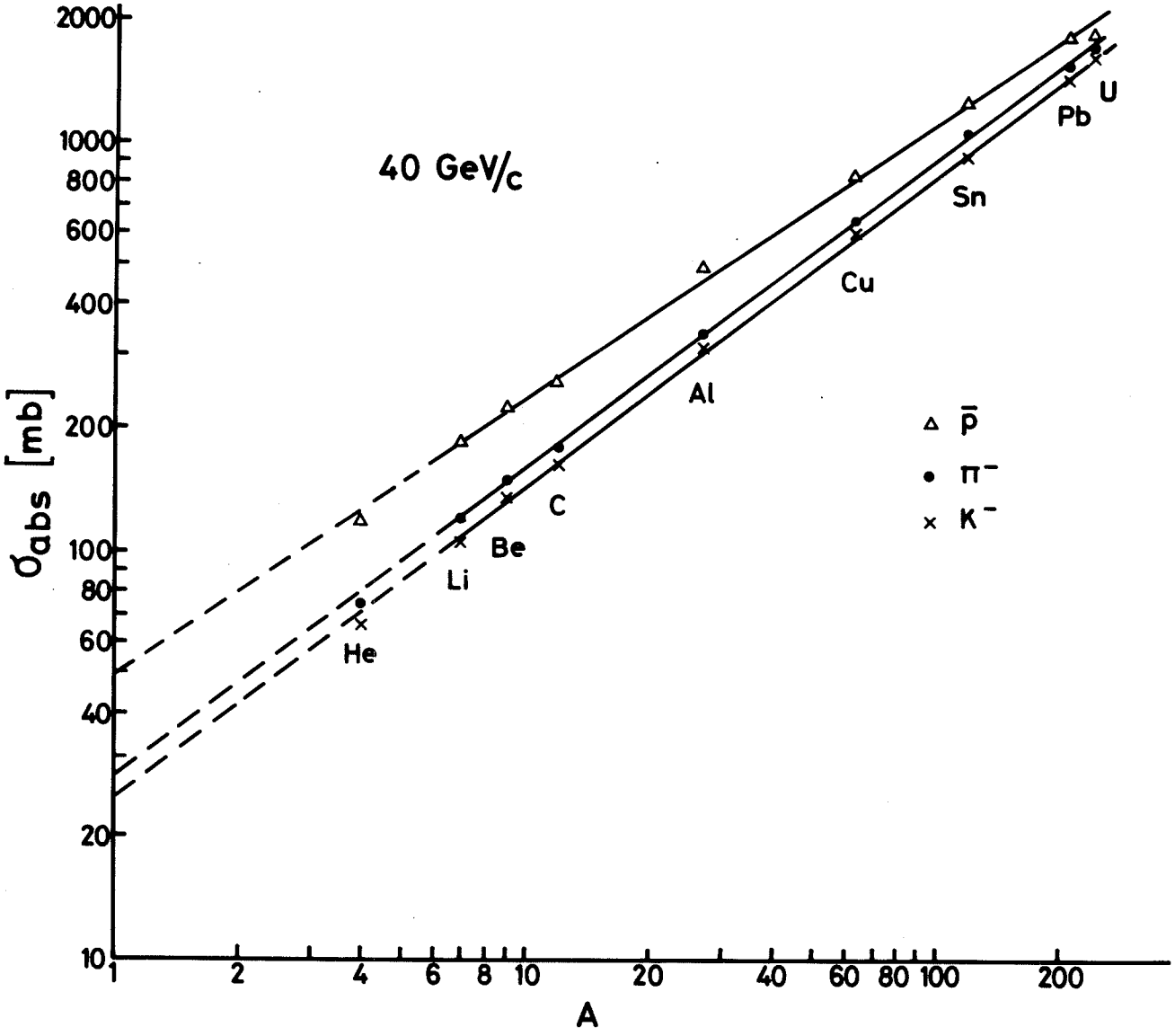
40 GeV/c
σ_{abs} [mb]
A
2000
1000
800
600
400
200
100
80
60
40
20
10
1
2
4
6
8
10
20
40
60
80
100
200
He
Li
Be
C
Al
Cu
Sn
Pb
U
$\bar{p}$
π^-
K^-

Fig:13